Dynamical Bond Formation in KNi2Se2

James Neilson, Allyson Fry-Petit, Natalia Drichko, Matthew Stone, Anna Llobet, Mahalingam Balasubramanian, Matthew R. Suchomel, Tyrel Mcqueen

Dynamical Bond Formation in KNi_2Se_2

James R. Neilson*[b], Allyson M. Fry-Petit[c], Natalia Drichko[d], Matthew B. Stone[e], Anna Llobet[f], Mahalingam Balasubramanian[g], Matthew R. Suchomel[h], and Tyrel M. McQueen*[a]

Dedicated to Mercouri Kanatzidis on his 65th birthday

Abstract: Emphanisis, or the appearance out of nothing, has been used to describe the phenomena of spontaneous atom off-centering and dipole formation at elevated temperatures in lead chalcogenides. Here, we provide spectroscopic evidence of spontaneous formation of metal-metal bonds above T ~ 50 K in the layered metal KNi_2Se_2. These bonds form zig-zag chains that lower the local symmetry from tetragonal to monoclinic. Energy-resolved pair distribution function measurements exclude a pure phonon origin of our observations, and instead imply the existence of extra, slowly fluctuating, Ni-Ni bonds above T = 50 K. Density functional theory calculations support this lower symmetry configuration as an instability of tetragonal KNi_2Se_2. We thus demonstrate that the phenomena of emphansis is not limited to local electric dipole formation, but can also be driven by the formation of metal-metal bonds.

[a] Prof. Tyrel M. McQueen
Department of Chemistry, Institute for Quantum Matter, William H. Miller III Department of Physics and Astronomy, Department of Materials Science and Engineering
Johns Hopkins University
3400 N. Charles St, Baltimore, MD 21218
E-mail: mcqueen@jhu.edu

[b] Dr. James R. Neilson
Department of Chemistry, Institute for Quantum Matter, Department of Physics and Astronomy
Johns Hopkins University
3400 N. Charles St, Baltimore, MD 21218
Present Address: Department of Chemistry, School of Advanced Materials Discovery, Colorado State University
Email: james.neilson@colostate.edu

[c] Dr. Allyson M. Fry-Petit
Department of Chemistry, Institute for Quantum Matter, Department of Physics and Astronomy
Johns Hopkins University
3400 N. Charles St, Baltimore, MD 21218
Present Address: Department of Chemistry, California State University, Fullerton

[d] Prof. Natalia Drichko
Institute for Quantum Matter, William H. Miller III Department of Physics and Astronomy
Johns Hopkins University
3400 N. Charles St, Baltimore, MD 21218

[e] Dr. Matthew B. Stone
Neutron Scattering Division, Oak Ridge National Laboratory, Oak Ridge, TN 37830

[f] Dr. Anna Llobet
Lujan Neutron Scattering Center, Los Alamos National Laboratory (LANL), Los Alamos, NM
Present Address: P-2: Dynamic imaging and radiography, LANL

[g] Dr. Mahalingam Balasubramanian
Advanced Photon Source
Argonne National Laboratory, Argonne, IL
Present Address: Electrification and Energy Infrastructure Division, Oak Ridge National Laboratory, Oak Ridge, TN

[h] Dr. Matthew R. Suchomel
Advanced Photon Source
Argonne National Laboratory, Argonne, IL
Present Address: Univ. Bordeaux, CNRS, Bordeaux INP, ICMCB, UMR 5026, F-33600, Pessac, France

Introduction

The structures of materials are generally described with crystallographic tools that assume the presence of point and translational symmetry operations, which are global properties of the system. Yet a material's structure is determined by the microscopic details and energetics of atoms coming together to form bonds – inherently local effects. Thus it should not be surprising that there are materials in which the global structure is only an average view, and distinct from the local structure. Indeed, many such materials are now known, as the tools to measure and quantify local symmetry have rapidly developed.[1]

One high profile and controversial example is the discovery of spontaneous off-centering of Pb ions as temperature is increased in the narrow gap semiconductor PbTe.[2] Termed emphanisis, this behavior is prima facie surprising since the normal expectation is that symmetry increases on warming (i.e. decreases on cooling as in, e.g. the Jahn-Teller effect, though there are exceptions[3]), whereas the opposite is observed in PbTe – there is a local decrease in symmetry at elevated temperature. Follow up work has shown that the local off-centering displacements are not random, but highly correlated[4], with similar behavior observed in other chalcogenides[5] and even halide perovskites[6].

We previously reported a similar phenomenon in KNi_2S_2 and KNi_2Se_2, with signatures of a charge density wave (CDW) in local structure measurements present at room temperature disappearing below T ≈ 50 K,[7,8] that stimulated further experimental and theoretical studies to understand the behavior.[9,10] Many questions remain, including the timescales on which the local symmetry lowering is present and the chemical driving force for the phenomenon.

Here we combine Raman spectroscopy, high resolution synchrotron X-ray diffraction and pair distribution function (PDF) analysis, Extended X-ray Absorption Fine Structure (EXAFS) spectroscopy, Dynamical (Energy-resolved) neutron PDF (DPDF) analysis, and Density Functional Theory to provide a substantially more complete picture of the symmetry lowering on warming in KNi_2Se_2, and find that it can be described as arising due to the spontaneous formation of Ni-Ni bonds to form zig-zag chains emerging from a square lattice of Ni atoms. It thus shares much phenomenology with the phenomena of emphansis previously reported in other contexts, but here driven by metal-metal bonding.

Results and Discussion

The high symmetry structure of KNi_2Se_2 is of the $ThCr_2Si_2$-type, Fig. 1a, and consists of $[Ni_2Se_2]^-$ layers of edge-sharing $NiSe_4$ tetrahedra separated by K^+ cations. Below T ≈ 10 K, an excellent

Rietveld refinement to the data is obtained for the previously reported *I4/mmm* structure, with the single crystallographically distinct nickel atom found on a 4d (0, 0.5, 0.25) Wyckoff site. However, above T > 50 K, the goodness-of-fit is improved by displacing the Ni atom from this ideal position to the 8g (0, 0.5, z) Wyckoff position with 50% fractional occupancy, as illustrated in the Fourier difference maps for T = 300 K in Fig. 1b. While there is no discontinuity in unit cell volume, Fig. 1c, the best fit model rapidly changes from 4d to 8g around T ~ 50 K, Fig. 1d. These data are suggestive of a local lowering of symmetry.

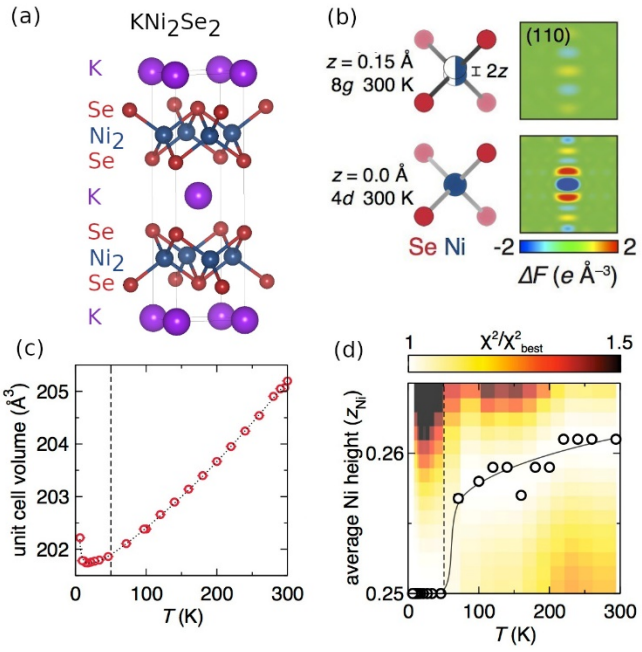

Figure 1. (a) The low temperature structure of KNi_2Se_2 (the c axis is vertically aligned). (b) At T = 300 K, a displacement of the Ni ions off the high symmetry 4d position to a split site 8g model is necessary to remove a systematic error in the electron density from synchrotron powder X-ray diffraction (SXRD). (c) Unit cell volume change from SXRD, showing no discontinuity at T = 50 K, even as (d) the structural model from SXRD changes from Ni centered (=0.25) to non-centered (>0.25). The background coloring shows the quantitative improvement of the model with the z-displacement at T > 50 K.

To further confirm this off-centering of Ni atoms, EXAFS measurements were performed at the Ni and Se *K*-edges, shown in Fig. 2a,b. Accompanying X-ray absorption spectroscopy (XAS, not shown) measurements from T = 300 to 8.5 K show no significant change in the formal valence of $Ni^{1.5+}$ or Se^{2-}, as neither edge moves in energy within the uncertainty of the XAS experiment (ΔE ~ 0.2 eV). However, there is a significant redistribution of the Fourier-transformed EXAFS signal for the Ni *K* edge as a function of temperature, indicative of a change in the Ni coordination environment. In contrast, there is no shift in the Se *K* edge EXAFS. The EXAFS is thus in agreement with the diffraction analysis that there are changes in the Ni atom positions as a function of temperature.

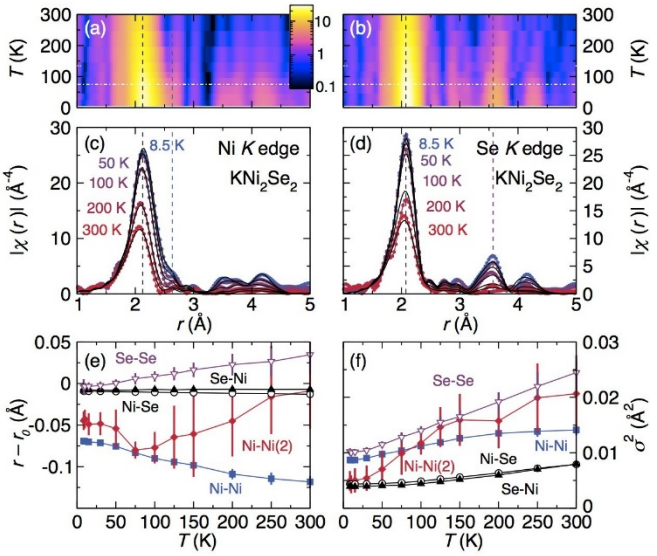

Figure 2. Temperature dependence of the EXAFS of KNi_2Se_2 measured at (a) the Ni *K* edge and (b) the Se *K* edge show a shift in spectral weight with temperature at the Ni *K* edge predominately around ~2.6 Å. Selected fits of (c) the Ni *K* edge and (d) the Se *K* edge EXAFS illustrate the better quality of fit of the tetragonal model below T < 75 K. (e) The temperature dependence of the shifts of different scattering path lengths illustrate that most of the changes reside on the Ni sublattice [paths: Ni-Se/Se-Ni r_0 = 2.40 Å; Ni-Ni r_0 = 2.76 Å; Se-Se and Ni-Ni(2) r_0 = 3.91 Å]. (f) The mean squared displacements of the path lengths indicate the same trend. Error bars are from the statistical error of the fit. The vertical bars at r ~ 2.1 Å indicate the Ni-Se or Se-Ni path length, Ni-Ni paths at r ~ 2.6 Å, and Se-Se paths at r ~ 3.6 Å.

The EXAFS data were quantitatively modeled using the average *I4/mmm* crystal structure to simulate the path lengths out to a cluster size of ~ 4.5 Å. The quality of fit of the model, as judged by the *R*-factor ($R = \sum(data - fit)^2 / \sum data^2$), is temperature independent from 8.5 K < T < 75 K (~ 0.7±0.1%); above that temperature the *R*-factor increases nearly linearly to 2.2% by T = 300 K. This reduced fit quality is also visible in Fig. 2c,d and indicates that the average crystal structure does not accurately describe the local Ni and Se environments for T > 75 K. Attempts to fit a distorted model to the higher temperature EXAFS were unreliable due to the correlation of multiple fitting parameters and the broadening of features in the data from enhanced thermal fluctuations. The temperature dependence of the path length changes (r-r_0) and mean-squared displacements (σ^2) obtained from the model fits give information on the general features of the local distortion.

The Ni-Se (Ni edge, Ni to Se path; 4x degenerate) and Se-Ni (Se edge, Se to Ni path; 4x degenerate) paths show very little temperature dependence, Fig. 2e, and the σ^2 exhibit the expected gradual increase on warming. The Se-Se path (Se edge, Se to Se nearest neighbor, r_0 ~ 3.91 Å) also does not show any temperature dependent inflections. In contrast, the Ni-Ni path (the 4x degenerate nearest-neighbor nickel separation, r_0 = 2.76 Å) has a significant temperature dependence, showing that the distance between the Ni atoms decreases on cooling from T = 300 K, saturating around T ~ 50 K, which is consistent with

the Ni atom position changes observed in Rietveld analysis of diffraction data. The next-nearest Ni-Ni separation (Ni-Ni(2), r_0 = 3.91 Å; 4x degenerate) shows an inflection at T = 75 K. While the significant error bars and increase in σ^2 prevent an accurate assignment of the exact disposition of that path length at higher temperatures, it is clear that the microscopic Ni environment changes at T ~ 75 K.

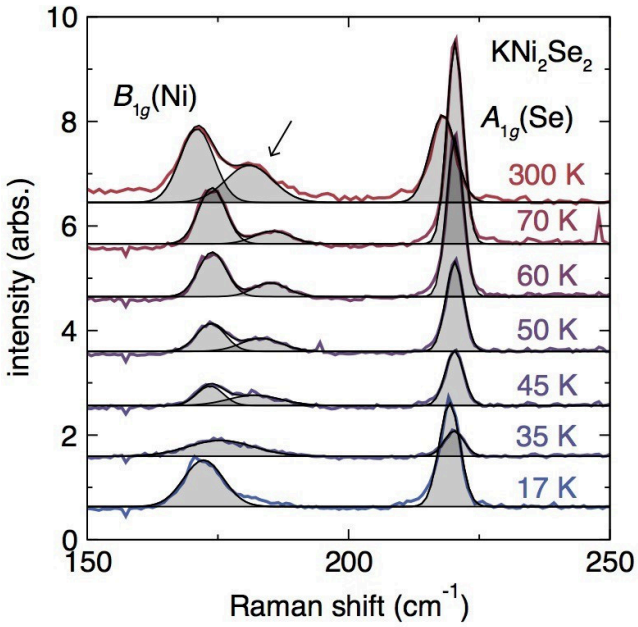

Figure 3. Temperature dependence of Raman spectra of KNi_2Se_2 collected perpendicular to the *ab* plane illustrate an additional phonon mode beyond that expected for the tetragonal *I4/mmm* space group (arrow) which softens into the neighboring B_{1g} (Ni) mode on cooling. Spectra are shifted along the y-axis for clarity.

Direct evidence for a formal local decrease in symmetry on temperature increase comes from Raman scattering measurements, Fig. 3. From a symmetry analysis of the low-temperature crystal structure (space group *I4/mmm*), we expect four Raman-active optical phonons.[11] In particular, Ni atoms in 4d Wyckoff positions contribute B_{1g} and E_g modes, of which only B_{1g} is observed in the *ab* plane. Se atoms in 4e Wyckoff positions show A_{1g} and E_g Raman active modes, of which only A_{1g} is observed in the *ab* plane. Indeed, the Raman spectra at T = 17 K, Fig. 3, shows two strong bands, located at 171 and 219 cm^{-1} (21.2 and 27.2 meV), which we assign to the B_{1g} (Ni) and A_{1g} (Se) vibrational modes respectively. The low temperature spectrum of KNi_2Se_2 has a shape very similar to the non-stoichiometric compound $K_{0.95}Ni_{1.86}Se_2$, for which no distortion is reported[10], even with somewhat higher phonon frequencies in the spectra of KNi_2Se_2.

On increasing the temperature above T ≈ 50 K, the lower-frequency Raman band shifts to higher frequencies, and another phonon becomes well-resolved at 186 cm^{-1}. This shape of the spectra persists to room temperature, and is direct evidence of a lowering of local point symmetry on warming. Further, this lowering of symmetry must be fluctuating on a timescale slower than that of the Raman measurement, ca. picoseconds (or not fluctuating at all).

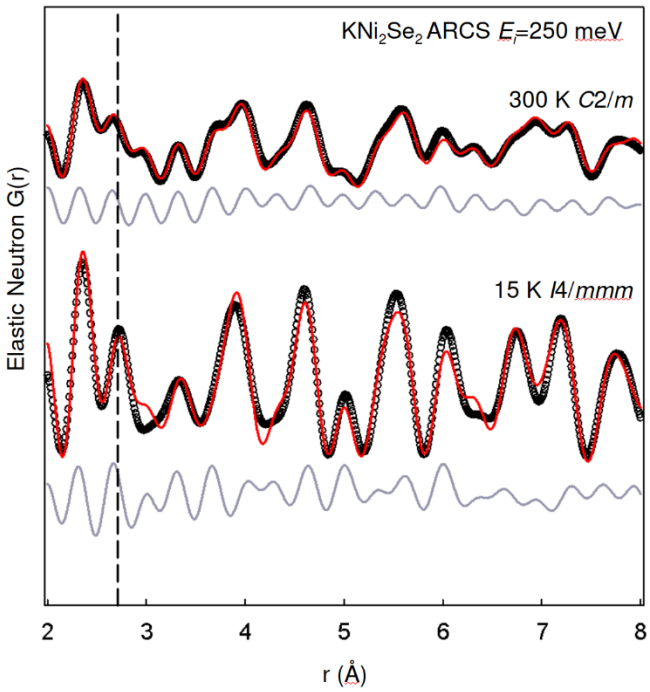

Figure 4. Energy-resolved (ΔE = 0 meV) pair distribution function data for KNi_2Se_2 collected at T = 15 K and T = 300 K. The single nearest-neighbor Ni-Ni distance (dashed line) is a single distance at T = 15 K, but broadens and splits into two distinct distances at T = 300 K, indicating a slowly fluctuating (or static) lowering of local symmetry. Red lines are models to the data, and gray lines are residuals.

Previous reverse Monte Carlo modeling of energy-integrated neutron PDF data[8] suggested the formation of Ni-Ni bond pairs at T > 50 K. However, such energy-integrated data also includes the contributions from phonon excitations (e.g. thermal diffuse scattering), making it challenging to disentangle phonon driven motions from additional local changes in symmetry beyond those driven by phonons. Further evidence that the local symmetry decrease above T ≈ 50 K is slowly fluctuating (or static) can come from an energy-resolved neutron PDF experiment that only selects elastically-scattered neutrons, avoiding contamination from phonon modes at energies higher than the instrumental energy resolution. Fig. 4 shows the G(r)'s obtained from an elastic neutron scattering experiment. The T = 15 K data is well-described by the previously reported high symmetry tetragonal structure of KNi_2Se_2. However, the T = 300 K cannot be adequately modeled with a tetragonal cell, but instead requires a lower symmetry *C2/m* model (vida infra).

To aid in determining the detailed local structure at T > 50 K, density functional theory (DFT) calculations were carried out. A

linear response DFT calculation of the zone center phonons for the low-temperature *I4/mmm* crystal structure of KNi_2Se_2 generally agrees with the results of Raman scattering measurements, Table 1, as well as with the mode energies and assignments reported in[10]. Calculation of the in-plane phonon dispersion, Fig. 5, reveals an imaginary frequency eigenvector at the *X* point in the Brillouin zone [q = (1/2 0 0), *E* = 5.2i meV].

Table 1. DFT calculated zone-center phonons for KNi_2Se_2 (*I4/mmm* space group).

Mode	Displacements	IR/R	DFT cm^{-1}	Meas cm^{-1}	Ref. 10 cm^{-1}
E_u	K(xy), Ni(xy), Se(zy)	IR	49.4		105.1
E_g	Ni(xy), Se(xy)	R	79.2		35.4
A_{2u}	K(z), Ni(z), Se(z)	IR	91.5		116.4
B_{1g}	Ni(z)	R	157.7	171	133.8
A_{1g}	Se(z)	R	188.9	219	189.4
E_u	K(xy), Ni(xy), Se(-xy)	IR	223.7		208.8
E_g	Ni(xy), Se(-xy)	R	229.6		203.9
A_{2u}	Ni(xy), Se(-xy)	IR	239.3		220.8

Imaginary frequency modes from DFT can be indicators of lattice instabilities, as exemplified by the localized, aperiodic distortions in $Bi_2Ti_2O_7$.[12] In the present case, this prediction for a distorted ground state contrasts with the experimentally observed undistorted tetragonal ground state at T < 50 K. However, this predicted lattice instability, Table 2, does resemble the distortion of KNi_2Se_2 above $T \approx 50$ K: the primary polarization components of the imaginary frequency eigenvector are out-of-plane Ni displacements [±z, with a small component along x, such that $z \approx 3x$], as illustrated in Fig. 5a, matching the findings of the diffraction and EXAFS analyses. Further, the computed vibrational density of states, Fig. 5b, matches well the phonon density of states from the inelastic neutron scattering measurement, after application of a small global scale factor.

Using ISODISTORT,[13] the imaginary-frequency zone-boundary phonon polarizations were decomposed into the subgroup symmetry *C2/m* (Table 2), which allowed for an excellent description of the elastic neutron PDF at $T = 300$ K, Fig. 4. Due to the large uncertainties associated with the low Q_{max} cutoff in the elastic neutron PDF experiment, we instead chose to obtain a final description of the room temperature structure by modeling room temperature X-ray total scattering data. Fits to the high-symmetry tetragonal structure, DFT X-point imaginary mode, and relaxed structure in *C2/m* are shown in Fig. 5c,d. The relaxed *C2/m* structure provides an excellent description of the X-ray PDF data, and final parameters for this structure are given in Table 2.

Table 2. Starting positions and directional components of the imaginary zone-boundary phonon [q = (1/2 0 0); E = 5.2i meV; *P-1* space group a = 3.89478 Å; b = 7.21191 Å; c = 7.78956 Å; α= 105.6657°, β = 90°, γ = 74.3343°] and also its refinement to the x-ray pair distribution function [space group *C2/m*; a = 13.92(6) Å; b = 3.90(4) Å; c = 7.8(1) Å; β = 105.9(7)°].

	Initial structure			Phonon components		
Atom	x	y	z	PIIa	PIIb	PIIc
K	0	0	0	0	0	0
Ni1	0.25	0.5	0.625	0.184	0	-0.599
Ni2	0.75	0.5	0.875	-0.184	0	0.599
Se1	0.649731	0.700538	0.675135	0.248	0	-0.214
Se2	0.350269	0.299462	0.824865	-0.248	0	0.214
	PDF refined structure (*C2/m*)					
Atom	x	y	z	U_{iso}		
K	0.49(1)	0	0.77(1)	0.03(2)		
Ni1	0.253(6)	0	0.87(1)	0.020(5)		
Ni2	0.259(6)	0	0.93(1)	0.016(4)		
Se1	0.851(4)	0	0.93(1)	0.016(4)		
Se2	0.858(3)	0	0.43(1)	0.016(4)		

The C2/m structure contains short and long Ni-Ni bonds, akin to the long-range ordered charge density wave (CDW) modulations in the structurally related compounds $SrRh_2As_2$ and KCu_2Se_2,[14] but in this case forming zig-zag chains. Yet, while the local bonding observed in PDF can be described by this lower symmetry monoclinic structure, the overall crystal symmetry determined by diffraction remains *I4/mmm*.

Thus we find the spontaneous and dynamic appearance of local Ni-Ni bonding in KNi_2Se_2 above $T \approx 50$ K that does not result in a change of the average structure. Simple electron counting provides a chemical insight into the origin of this behavior: due to charge transfer from the potassium ions, there is one extra electron for each pair of Ni atoms, or, equivalently, two extra electrons for every four Ni atoms, in the material. These extra electrons then occupy Ni-Ni antibonding orbitals[15] and drive the lengthening of Ni-Ni bonds where these electrons localize, and concomitant slight reductions in distances for Ni-Ni bonds where the electrons are not localized. If there were twice this number of extra electrons, as in KCu_2Se_2, the formation of 1D chains of transition metal ions is expected. In the case of KNi_2Se_2, however, there are insufficient electrons to form such an ordered lattice. Instead, it appears that the ground state does not localize electrons into such antibonding states. However, such a state is still nearby in energy, and the addition of temperature is sufficient to drive the population of antibonding states and formation of Ni-Ni (anti)bonds – most plausibly attributed to the entropy gain associated with their formation. This thus precisely resembles the

emphanisis reported in dipole former (e.g. Pb^{2+}) materials, but driven by Ni-Ni (anti)bond formation.

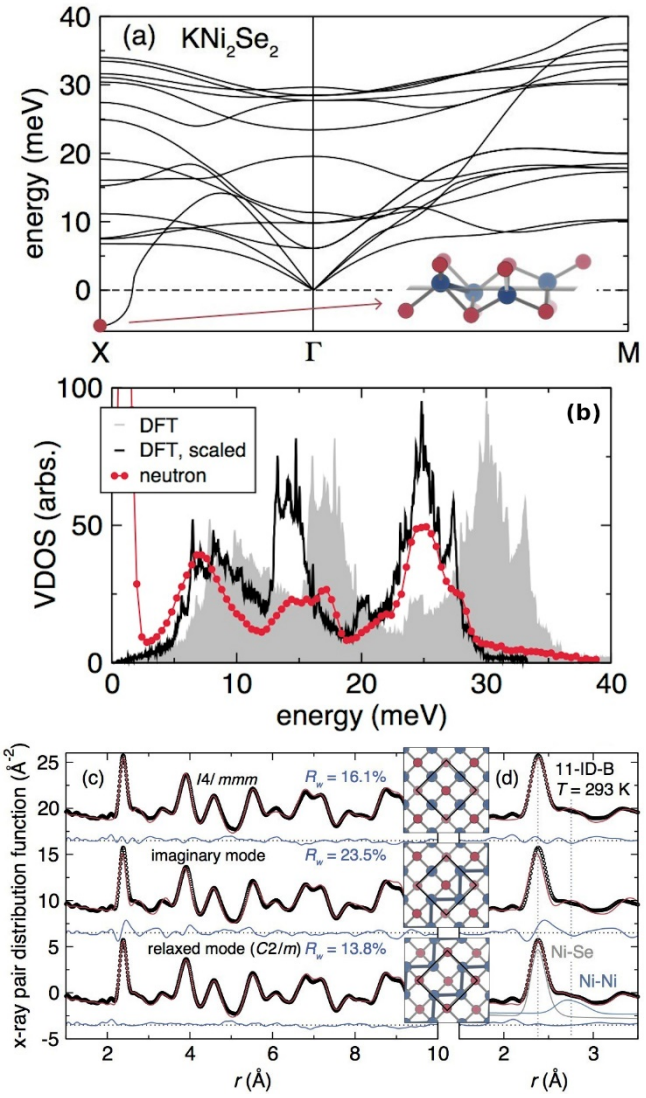

Figure 5. (a) DFT calculated phonon dispersion curves with a negative energy mode [q = (1/2 0 0)]; the illustrated mode corresponds to out-of-plane Ni displacements [Ni: blue (dark) circles; Se: red (light) circles; amplitude exaggerated for clarity]. (b) Calculated vibrational density of states (VDOS) compared to that measured via inelastic neutron scattering. (c) X-ray pair distribution function (PDF) of KNi_2Se_2 (T = 300 K; filled circles; reproduced and offset for clarity). Lines through the data are the calculated PDF from the *I4/mmm* crystal structure (top), the imaginary frequency eigenvector from the DFT phonon calculation (middle), and its least-squares relaxation within space group symmetry *C2/m* (bottom); differences are below. (d) Illustration of Ni-Se and Ni-Ni pairwise correlations. Insets illustrate the corresponding [Ni_2Se_2] plane (bonds denote nearest neighbors).

Conclusions

Through a combination of spectroscopic probes and DFT calculations, here we report on the spontaneous formation of local Ni-Ni (anti)bonds above T ≈ 50 K in KNi_2Se_2. We thus find that the previously reported symmetry decrease on warming in KNi_2Se_2 can be described as arising due to the spontaneous formation of such Ni-Ni (anti)bonds emerging from a square lattice of Ni atoms. It thus shares much phenomenology with the phenomena of emphansis previously reported in other contexts, but here driven by metal-metal bonding.

Experimental Section

Microcrystalline specimens of KNi_2Se_2 were prepared and manipulated as previously described.[8,15] Raman spectra were obtained from the *ab* plane of single micro-crystals in a parallel-sided fused silica capillary (evacuated to p_{He} = 10 torr at RT) at temperatures between T = 300 and 17 K using a T64000 Jobin-Yvone spectrometer equipped with an Olympus microscope and LN2 cooled CCD using a 2 μm probe, λ = 647 nm from a Ar-Kr Spectra-Physics laser. Low-temperature measurements were performed using a Janis ST-300 He-flow cryostat. The laser power was below 0.3 mW to avoid sample heating, which was estimated by comparing Stokes and anti-Stokes spectra at T = 200 K. High-resolution synchrotron X-ray diffraction data, collected at the Advanced Photon Source (APS) on beamline 11-BM.[7,16] Rietveld analysis were performed using GSAS/EXPGUI.[17] Pair distribution function analysis was carried out using PDFGUI.[18] XAS and EXAFS were performed at the APS on beamline 20-BM-B with powder specimens immobilized in BN pellets measured in transmission using a closed-cycle cryostat. Calibration to Ni foil, normalization, and analysis of the EXAFS were all performed using ATHENA, and fits to the EXAFS were performed using the IFEFFIT code implemented in ARTEMIS.[19] DFT calculations were performed using Elk[20] with the spin-polarized PBEsol GGA functional[21] and the default full potential linearized augmented place wave (FP-LAPW) basis set with local orbitals specified for K, Ni, and Se. All calculations were performed on the experimentally determined reduced primitive unit cell (lattice parameters determined at base temperature) with an 8x8x4 k-point mesh and converged to better than $5.0 \cdot 10^{-5}$ Ha in energy and $5.0 \cdot 10^{-6}$ RMS change in Kohn-Sham potential. Non-magnetic, ferromagnetic, and antiferromagnetic configurations were tested, and the non-magnetic one found to be lowest in energy. The only variable internal coordinate, the z position of Se, was optimized so that the calculated forces were less than $5.0 \cdot 10^{-5}$ Ha; the change in Se z-position from the experimental value was less than 0.005 relative lattice units. Linear response phonon calculations were carried out over a 2x2x1 q-point mesh with atom displacements of 0.005 relative lattice units. Convergence of all calculations was checked with respect to the number of k-points, angular momentum cutoffs, and number of empty orbitals included. Elastic neutron PDF and vibrational density of states (VDOS) for KNi_2Se_2 were obtained from neutron scattering measurements using the ARCS spectrometer.[22] For VDOS, a powder sample was loaded in a 0.375" Al can under helium gas, approximately 2/3rd full, with an incident collection energy of E_i = 40 meV. The empty can signal was subtracted during analysis. For PDF, a powder sample with an atmosphere of helium gas was loaded in a thin walled annular vanadium can with outer diameter 1.5", wall thickness 0.005", and 2.5 mm thickness between the inner annulus and OD to limit multiple scattering. Data was acquired with Ei = 250 meV neutrons. Data from an empty annular can was collected under the same experimental conditions and subtracted during analysis. Data from neutron energy transfers within 5 meV of the elastically scattered neutrons were used to perform the PDF

analysis. Initial data reduction and extraction of the neutron weighted vibrational density of states was performed in Mantid,[23] with subsequent reduction and analysis of PDF data in PDFGUI.[18]

Acknowledgements

We thank James Murray and Zlatko Tesanovic for inspiration and motivation, Igor Mazin for helpful discussions, Kevin Bayer and Karena Chapman for data collection at 11-ID-B, and Collin Broholm, Martin Mourigal, and W. Adam Phelan for help with the ARCS experiments. We thank W. Dmowski and T. Egami for use of their annular vanadium can. This research and the Raman spectrometer are principally supported by the US Department of Energy (DoE), Office of Science, Office of Basic Energy Sciences (BES), Division of Materials Sciences and Engineering under award DE-FG02-08ER46544, as well as funding from the David and Lucile Packard Foundation. This research has benefited from the use of beamlines 11-BM-B, 11-ID-B, and 20-BM-B at the Advanced Photon Source at Argonne National Laboratory, supported by the US. DoE, Office of Science, Office of Basic Energy Sciences, under Contract No. DE-AC02-06CH11357. Some initial work was performed at the Lujan Center at the Los Alamos Neutron Science Center, funded by the Office of Basic Energy Sciences of the US DoE. The Los Alamos National Laboratory was operatedby Los Alamos National Security LLC under DOE contract DE-AC52-06NA25396. A portion of this research used resources at the Spallation Neutron Source, a DOE Office of Science User Facility operated by the Oak Ridge National Laboratory.

Keywords: emphansis • metal-metal bonding • pair distribution function • raman scattering • diffraction

[1] T. Egami, S.J.L. Billinge, *Underneath the Bragg peaks: Structural Analysis of Complex Materials (Volume 16)*, Pergamon Materials Series, 2nd Ed., Pergamon (Elsevier), New York, **2013**.

[2] a) K.M.Ø. Jensen, E.S. Božin, C.D. Malliakas, M.B. Stone, M.D. Lumsden, M.G. Kanatzidis, S.M. Shapiro, S.J.L. Billinge, *Phys. Rev. B* **2012**, 86, 085313. b) E.S. Božin, C.D. Malliakas, P. Souvatzis, T. Proffen, N.A. Spaldin, M.G. Kanatzidis, S.J.L. Billinge, *Science* **2010**, 330, 1660-3.

[3] a) J.Schneck, J.Primot, R.Von der Mühll, J.Ravez, *Solid State Communications* **1977**, 21, 57-60. b) S.A.J. Kimber, J.A. Rodgers, H. Wu, C.A. Murray, D.N. Argyriou, A.N. Fitch, D.I. Khomskii, and J.P. Attfield, *Phys. Rev. Lett.* **2009**, 102, 046409.

[4] B. Sangiorgio, E.S. Bozin, C.D. Malliakas, M. Fechner, A. Simonov, M.G. Kanatzidis, S.J.L. Billinge, N.A. Spaldin, T. Weber, *Phys. Rev. Mater.* **2018**, 2, 085402.

[5] M. Dutta, K. Pal, M. Etter, U.V. Waghmare, K. Biswas, *J. Am. Chem. Soc.* **2021**, 143, 16839-48.

[6] G. Laurita, D.H. Fabini, C.C. Stoumpos, M.G. Kanatzidis, R. Seshadri, *Chem. Sci.* **2017**, 8, 5628-35.

[7] J.R. Neilson, A. Llobet, J. Wen, M.R. Suchomel, T.M. McQueen, *Phys. Rev. B* **2013**, 87, 216402.

[8] J.R. Neilson, A. Llobet, A.V. Stier, L. Wu, J. Wen, J. Tao, Y. Zhu, Z.B. Tesanovic, N.P. Armitage, T.M. McQueen, *Phys. Rev. B* **2012**, 86, 054512.

[9] a) J.M. Murray, Z. Tesanovic, *Phys. Rev. B* **2013**, 87, 081103. b) H. Lei, M. Abeykoon, K. Wang, E.S. Bozin, H. Ryu, D. Graf, J.B. Warren, C. Petrovic, *Journal of Physics Condensed Matter* **2014**, 26, 015701. c) H. Wang, C. Dong, Q. Mao, R. Khan, X. Zhou, C. Li, B. Chen, J. Yang, Q. Su, M. Fang, *Phys. Rev. Lett.* **2013**, 111, 207001. d) H. Wang, Q. Mao, H. Chen, Q. Su, C. Dong, R. Khan, J. Yang, B. Chen, M. Fang, *Journal of Physics Condensed Matter* **2015**, 27, 395701. e) F. Hardy, A. E. Böhmer, D. Aoki, P. Burger, T. Wolf, P. Schweiss, R. Heid, P. Adelmann, Y. X. Yao, G. Kotliar, J. Schmalian, C. Meingast, *Phys. Rev. Lett.* **2013**, 111, 027002. f) V. Stanev, P.B. Littlewood, *Phys. Rev. B* **2013**, 87, 161122. g) V. Bannikov, A. Ivanovskii, *Physica B: Cond. Matt.* **2013**, 418, 76. h) F. Lu, J.Z. Zhao, W.-H. Wang, *Journal of Physics Condensed Matter* **2012**, 24, 495501. i) V. Bannikov, A. Ivanovskii, *Physica C: Superconductivity* **2013**, 492, 44-8.

[10] N. Lazarević, M. Radonjić, M. Šćepanović, Hechang Lei (雷和畅), D. Tanasković, C. Petrovic, and Z. V. Popović, *Phys. Rev. B* **2013**, 87, 144305.

[11] D. Orobengoa, C. Capillas, M.I. Aroyo, J.M. Perez-Mato, *J. Appl. Cryst.* **2009**, 42, 820.

[12] D.P. Shoemaker, R. Seshadri, A.L. Hector, A. Llobet, T. Proffen, C.J. Fennie, *Phys. Rev. B* **2010**, 81, 144113.

[13] B.J. Campbell, H.T. Stokes, D.E. Tanner, D.M. Hatch, *J. Appl. Cryst.* **2006**, 39, 607.

[14] a) V. Zinth, V. Petricek, M. Dusek, D. Johrendt, *Phys. Rev. B* **2012**, 85, 014109. b) O. Tiedje, E.E. Krasovskii, W. Schattke, P. Stoll, C. Nather, W. Bensch, *Phys. Rev. B* **2003**, 67, 134105.

[15] J.R. Neilson, T.M. McQueen, *J. Am. Chem. Soc.* **2012**, 134, 7750.

[16] J. Wang, B.H. Toby, P.L. Lee, L. Ribaud, S.M. Antao, C. Kurtz, M. Ramanathan, R.B.V. Dreele, M.A. Beno, *Rev. Sci. Instrum.* **2008**, 79, 085105.

[17] a) A.C. Larson, R.B.V. Dreele, Los Alamos National Laboraotry Report LAUR 86-748 **2004**. b) B.H. Toby, *J. Appl. Cryst.* **2001**, 34, 210.

[18] C.L. Farrow, P. Juhas, J.W. Liu, D. Bryndin, E.S. Božin, J. Bloch, T. Proffen, S.J.L. Billinge, *Journal of Physics Condensed Matter* **2007**, 19, 335219.

[19] a) B. Ravel, M. Newville, *J. Synch. Rad.* **2005**, 12, 537. b) M. Newville, *J. Synch. Rad.* **2001**, 8, 322.

[20] The Elk Code, https://elk.sourceforge.net

[21] J.P. Perdew, A. Ruzsinszky, G.I. Csonka, O.A. Vydrov, G.E. Scuseria, L.A. Constantin, X. Zhou, K. Burke, *Phys. Rev. Lett.* **2008**, 100, 136406.

[22] E.S. Bozin, P. Juhas, W. Zhou, M. B. Stone, D.L. Abernathy, A. Huq, S.J.L. Billinge, *J. Appl. Cryst.* **2009**, 42, 724-725.

[23] The Mantid Project, https://www.mantidproject.org